colloids and interfaces

MDPI

Article

Synthesis of Chitosan Nanocomposite Materials Grafted with MWCNTs for the Removal of Tetracycline Pharmaceutical from Water Samples

Milton Shabeng Kgoete, Conny Putsane Mokgohloa and Lutendo Evelyn Macevele *

Department of Chemistry, University of Limpopo, Private Bag X1106, Sovenga 0727, South Africa; conny.mokgohloa@ul.ac.za (C.P.M.)

* Correspondence: lutendo.macevele@ul.ac.za; Tel.: +27-15-268-3691

Abstract

Pharmaceutical contaminants such as tetracycline pose an increasing threat to aquatic ecosystems and human health as a result of their persistence in water sources and their contribution to antibiotic resistance. This study developed chitosan nanocomposites by incorporating functionalised and nitrogen-doped multi-walled carbon nanotubes (FMWCNTs and NMWCNTs) for the removal of tetracycline pharmaceutical contaminants from water. The composites were characterised with FTIR, SEM, XRD, BET, UV–Vis, and TGA under various conditions (pH, adsorbent dosage, concentration, contact time, and temperature). Optimal tetracycline removal (85%) was achieved with pH 6, 2 g/L adsorbent dose, 10 ppm concentration, and 30 min contact time. The FMWCNT–chitosan composite could be recycled five times with an adsorption loss of only 2%. The FMWCNT–chitosan composite showed the good adsorption efficiency of 82% in the presence of counter ions and 70% in a binary system. The adsorption process followed the Langmuir isotherm (263 mg/g), indicative of monolayer adsorption and pseudo-second-order kinetics. Among the nanocomposites prepared, the FMWCNT–chitosan composite showed the highest performance, removing more than 85% of tetracycline from water samples.

Keywords: FMWCNTs; NMWCNTs; chitosan; adsorption; tetracycline

Academic Editor: Abhijit Dan

Received: 12 May 2025
Revised: 24 July 2025
Accepted: 27 July 2025
Published: 14 October 2025

Citation: Kgoete, M.S.; Mokgohloa, C.P.; Macevele, L.E. Synthesis of Chitosan Nanocomposite Materials Grafted with MWCNTs for the Removal of Tetracycline Pharmaceutical from Water Samples. *Colloids Interfaces* **2025**, *9*, 69. https://doi.org/10.3390/colloids9050069

1. Introduction

Water resources and supply systems are under increasing pressure due to increasing demand and the deterioration of quality in many water sources [1]. Most often, the water source is raw water from rivers and lakes. Unfortunately, untreated wastewater and industrial effluents are exposed to these water sources [2]. Pharmaceutical contaminants are increasingly recognised as a significant threat to water quality due to their widespread use and persistence in the environment [3,4]. These substances, including antibiotics, painkillers, and hormones, frequently enter aquatic systems through wastewater release, agricultural runoff, and inadequate disposal methods [2]. Pharmaceuticals may have detrimental effects on aquatic ecosystems and human health even at low levels, leading to problems such as antibiotic resistance and bioaccumulation within the food chain [5,6].

Between 2004 and 2009, a study conducted by the United States Geological Survey (USGS) revealed that pharmaceutical manufacturing facilities can contribute significantly to environmental pharmaceutical contamination [7]. An analysis of effluents from two wastewater treatment plants that processed discharges from pharmaceutical manufacturing

facilities revealed that the pharmaceutical concentrations were significantly higher, ranging from 10 to 1000 times, compared to the effluents from twenty-four other wastewater treatment plants nationwide that did not handle such discharges [7]. Tetracycline, a broad-spectrum antibiotic, inhibits protein synthesis and is widely used in medicine and agriculture [8]. Its persistence in water and soil makes it a significant environmental contaminant that contributes to antibiotic resistance and disrupts ecosystems. It enters these ecosystems through wastewater, agricultural runoff, and improper disposal [9]. When present in drinking water, it poses serious public health risks by promoting the growth of resistant bacteria and potentially disturbing the intestinal microbiota [10,11]. This highlights the need for better water treatment and stricter regulations to mitigate its impact on human health and the environment.

Various techniques have been developed to improve wastewater quality including nanofiltration, electrolysis, reverse osmosis, photocatalysis, biodegradation, and adsorption [3,12,13]. However, these approaches often come with drawbacks, such as high operational costs and environmental risks posed by hazardous chemicals [14]. Researchers have placed great emphasis on adsorption due to its high effectiveness, low cost, and simplicity of use, as well as the variety of available adsorbents, such as inorganic, organic, and biosorbent materials [15,16]. Chitosan, a biodegradable biopolymer derived from chitin, is a promising material for water purification due to its eco-friendliness, non-toxicity, and the ability to form effective interactions with various pollutants [17–19]. Dey et al. [20] evaluated the performance of chitosan as an adsorbent for Remazol Red. The study focused on evaluating the ability of chitosan to remove Remazol Red, a synthetic dye, from aqueous solutions, which is crucial in wastewater treatment. The findings showed that, under ideal conditions, chitosan had excellent adsorption characteristics and demonstrated substantial potential as an environmentally acceptable and efficient adsorbent for the elimination of pollutants from aqueous solutions [20].

The adsorption efficiency of chitosan can be significantly enhanced by integrating it with nanomaterials such as multi-walled carbon nanotubes (MWCNTs) due to their high surface area, excellent electrical and thermal conductivity, high mechanical strength, and the capability to be functionalised for specific water contaminant removal [19,21,22]. Furthermore, doping multi-walled carbon nanotubes with nitrogen offers numerous benefits in water treatment, mainly due to their improved adsorption capacity and catalytic activity [23]. By combining the natural adsorptive qualities of chitosan with the large surface area and stability of the nanoparticles, the chitosan-based nanocomposites are more efficient in removing pharmaceutical pollutants from aqueous environments [15,24].

A study of adsorption isotherms for the removal of tetracycline from water using carbon mineral compounds determined by inverse liquid chromatography has shown that the highest amount of adsorbed tetracycline is 19.1 mg/g [25]. Yu et al. [26], in a study on the enhanced removal of tetracycline from water using a MgO-modified g-C_3N_4 composite, achieved 85% tetracycline removal within 90 min, and the composite maintained a removal efficiency above 70% after six cycles. These studies, among others, highlight the potential of advanced nanocomposite materials to mitigate tetracycline contamination in aquatic systems. Table 1 presents additional materials that have been developed for this purpose. However, a composite offers a low-cost, biodegradable, and easily recoverable alternative with high adsorption efficiency and excellent recyclability across multiple cycles.

Table 1. Various adsorbent materials are used in the adsorption of tetracycline from water samples.

Adsorbent	Adsorption Capacity	Contact Time	References
Activated carbon	17.88 mg/g	400 min	[27]
MWCNTs doped with polypyrrole	34.50 mg/g	60 min	[28]
Raw shrimp shell waste (SSW)	229.98 mg/g	36 h	[29]
Geo-Material	12.58 mg/g	30 min	[30]
CS·Fe_3O_4	211.21 mg/g	180 min	[31]
Natural Iraqi bentonite	23.69 mg/g	120 min	[32]
Fe/Cu–GO	201.9 mg/g	15 min	[33]
Fe–HAP	45.39 mg/g	45 min	[34]
Z–HAP–AA	244.63 mg/g	600 min	[35]

This study investigates the synthesis of chitosan nanocomposites, particularly those that incorporate MWCNTs, to evaluate their potential for removing tetracycline as a pharmaceutical pollutant from drinking water. The objective is to evaluate their adsorption capacity and effectiveness, with a focus on their applicability for pharmaceutical water treatment.

2. Materials and Methods

2.1. Materials

Analytical-grade materials and chemicals were used without further purification. The primary material for the study was tetracycline, a commonly used antibiotic. Glutaraldehyde served as a cross-linking agent. Additional chemicals, including sodium hydroxide (NaOH), sulfuric acid (H_2SO_4), acetic acid (CH_3COOH), MWCNTs, and chitosan flakes, were obtained from Sigma-Aldrich (St. Louis, MO, USA). Nitrogen-doped multi-walled carbon nanotubes (NMWCNTs) were purchased from SabiNano (PTY) Ltd. (Randburg, South Africa). Deionised water was used to prepare all the solutions.

2.2. Functionalisation of MWCNTs

To functionalise MWCNTs, the process was carried out in a 250 mL beaker using a solution of 10 mL of nitric acid and 30 mL of sulfuric acid following a method described previously [22]. After adding a gram of MWCNTs, the mixture was sonicated for three hours. Following sonication, deionised water was used to dilute the solution followed by filtration and washing until the pH reached 7. Subsequently, the MWCNTs were dried for 24 h in an oven (EcoTherm Economy Oven, Labotec (Pty) Ltd., Midrand, South Africa) from at 80 °C and weighed.

2.3. Preparation of Chitosan Beads

In order to produce chitosan beads, the chitosan flakes were dissolved in 150 mL of 5% CH_3COOH solution as previously described [4]. The solution was added dropwise to a beaker with 500 mL of 0.50 M NaOH after being agitated overnight. A magnetic stirrer (Model E-MS3-H2D, EINS SCI Co., Ltd., Seoul, South Korea) was used for continuous stirring at 200 rpm during dropwise addition, ensuring that the acetic acid in the chitosan gel was neutralised, which caused the gel to coagulate into uniform spherical chitosan beads. The chitosan beads were then filtered and washed with 200 mL of distilled water, after which they were left overnight in 110 mL of 0.025% glutaraldehyde solution at room temperature. The beads were then filtered and washed with an additional 200 mL of deionised water. Finally, the chitosan beads were dried for 24 h at 40 °C and ground to powder.

2.4. Preparation of 1% Functionalised MWCNT–Chitosan Composite

In a 250 mL beaker, 2 g of chitosan flakes was dissolved in 120 mL of 5% acetic acid solution to produce functionalised MWCNT–chitosan composites. Next, 0.02 g of MWCNTs was added to 30 mL of the 5% acetic acid, and the mixture was sonicated for 25 min. The two solutions were then combined and stirred overnight before being added dropwise to a beaker containing 500 mL of 0.50 M. Acetic acid in the chitosan gel was neutralised using a magnetic stirrer at 200 rpm to continuously swirl the mixture during dropwise addition. This resulted in the gel coagulating into homogeneous spherical chitosan beads. After filtering, 200 mL of distilled water was used to wash the chitosan beads. At room temperature, they were left overnight in 110 mL of a 0.025% glutaraldehyde solution. The beads were washed with 200 mL of deionised water and filtered again. Finally, the chitosan beads were dried for 24 h at 40 °C and ground into a powder.

Nitrogen-doped MWCNTs were prepared in the same manner as described above.

2.5. Characterisation

Fourier transform infrared (FTIR) spectroscopy was performed using a PerkinElmer Spectrum 100 spectrometer (PerkinElmer Inc., Shelton, CT, USA) to identify the formation of the samples and functional groups within the range of 4000–500 cm^{-1}. The morphological structure of the synthesised nanoparticles was examined using a sigma 500 VP Scanning Electron Microscopy (SEM) from (Carl Zeiss Microscopy GmbH, Köln, Germany). The images were provided at a resolution of 1024 × 768 pixels, with varying magnifications applied to each composite sample to facilitate a clearer identification. X-ray diffraction patterns to assess the phases, crystallinity, and crystallite sizes were recorded using a Cu Kα radiation source (λ_1 = 1.540598 Å, λ_2 = 1.544426 Å; $K\alpha_2/K\alpha_1$ intensity ratio = 0.5). The instrument was operated at 30 kV and 10 mA, without the use of a monochromator. Data were collected over a 2θ range of 5.01° to 89.99. The TGA was carried out using TGA Q500 (version 20.13, build 39) from (TA Instruments, New Castle, DE, USA), operated in ramp mode up to 900 °C at a heating rate of 10 °C/min. The analysis was conducted under a mixed-gas atmosphere using an EGA-type furnace. Nitrogen served as the balance purge gas at a flow rate of 10.0 mL/min, while air was used as the sample/reactive gas at 90.0 mL/min. BET analysis was performed on a Micromeritics ASAP 2020 instrument (Micromeritics Instrument Corp., Norcross, GA, USA), and the samples were degassed at 40 °C for 16 h to investigate the surface properties of the nanocomposite membranes.

2.6. Batch Adsorption Studies of Tetracycline

The removal of tetracycline using a chitosan nanocomposite was investigated by altering various experimental parameters, such as the pH (3 to 8, adjusting the pH with 0.1 M NaOH and 0.1 HCl), adsorbent dosage (1 to 5 g/L), contact time (5 to 120 min and after 1440 and 2880 min), and concentration (10 to 50 ppm). The samples were rapidly examined using Nanocolor UV/Vis II Spectrophotometer (Macherey-Nagel GmbH & Co. KG, Düren, Germany) after each trial, followed by filtering using filter paper to eliminate suspended solids. All adsorption experiments were conducted in duplicate. The mean and standard deviation were calculated from the two measurements, and error bars representing the standard deviation were included in the graphs to reflect the experimental variability.

Equation (1) is the formula for calculating the percentage of tetracycline removal.

$$Removal\ \% = \frac{C_o - C_e}{C_o} \times 100 \quad (1)$$

Equation (2) yields the adsorption capacity, q_e (mg/g) of the adsorbent.

$$q_e = \frac{(C_o - C_e)V}{W} \quad (2)$$

- Co (mg/L) is the initial concentration of the tetracycline concentration.
- W (g/L) is the concentration of the adsorbent.
- C (e) (mg/L) is the equilibrium concentration of tetracycline.
- V (L) is the volume of tetracycline solution.

Adsorption Mechanism

The adsorption of tetracycline by chitosan nanocomposite works through a combination of π–π interactions, hydrogen bonding, and electrostatic forces. Once the adsorbent is added to the contaminated water, tetracycline molecules interact with the surface of the adsorbent through multiple pathways. As shown in Figure 1 on, π–π stacking interactions arise from the alignment of tetracycline's aromatic rings with the extended π–electron networks present on the carbon-based components of the nanocomposite, such as functionalized multi-walled carbon nanotubes. Functional groups on the chitosan, like -OH and -NH_2, engage with the polar functional groups of tetracycline to allow hydrogen bonding. At pH 6, the amino groups in chitosan become protonated, giving the surface a positive charge, while tetracycline predominantly exists in a neutral or mildly negative state. This charge difference facilitates electrostatic attraction.

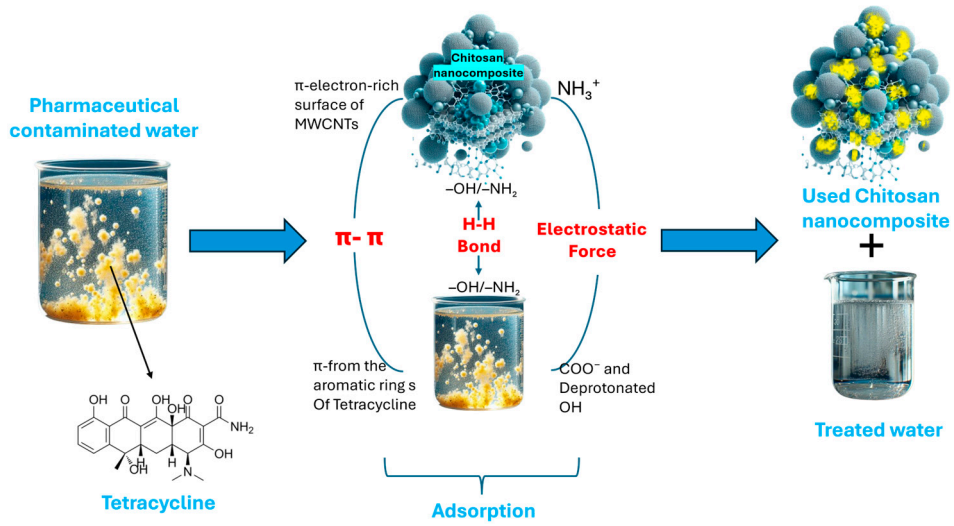

Figure 1. Adsorption mechanism of adsorption of pharmaceuticals by chitosan nanocomposite.

2.7. Reusability

To investigate the efficiency of the synthesised material and its cost-effectiveness, reusability studies were conducted under the acquired optimum adsorption parameters. These were carried out by performing five cycles of tetracycline adsorption–desorption tests for 30 min at 25 °C; 0.2 g/L of each adsorbent was contacted with 20 mL of tetracycline solution (10 ppm). Following adsorption, the adsorbents were regenerated by submerging each separately in 50 mL of 0.1 M NaOH solution for 2 h at 25 °C to desorb tetracycline. After that, deionised water was used to properly wash the adsorbents to remove NaOH.

2.8. Ionic Strength

The effect of ionic strength on the adsorption performance of the best-performing composite, FMWCNT–chitosan, was investigated under conditions designed to simulate

real water matrices. The experiment was carried out at pH 6, with an adsorbent dosage of 2 g/L, a contact time of 30 min, and a temperature of 25 °C, using a 10 ppm tetracycline solution containing sulphate (50 mg/L), nitrate (5 mg/L), and chloride (60 mg/L).

2.9. Binary System

To investigate the interference effect of one drug on another, a binary solution containing 10 ppm of tetracycline and tylosin was prepared. The adsorption experiment was conducted at pH 6, using 2 g/L of the FMWCNT–chitosan composite (the best-performing adsorbent), with a contact time of 30 min at 25 °C.

2.10. Kinetic Modeling of Adsorption

The pseudo-first-order kinetics are as follows:

$$In(q_e - q_t) = Inq_e - K_1 t \quad (3)$$

where

- q_t is the adsorbed adsorbate at time (t) (mg/g);
- q_e represents the equilibrium adsorption amount (mg/g);
- K_1 is the rate constant of adsorption (min^{-1}), which is found by plotting ln ($q_e - q_t$) versus time (t).

Pseudo-second-order kinetics are as follows:

$$\frac{t}{q_t} = \frac{1}{K_2 q_e^2} + \frac{t}{q_e} \quad (4)$$

where

- K_2 is the rate constant for pseudo-second-order sorption (g/mg·min);
- q_t represents the amount of adsorbed adsorbate at time t (mg/g);
- q_e represents the equilibrium amount of adsorption (mg/g).

2.11. Adsorption Isotherm Modeling

(a) Langmuir

This is an empirical model derived from kinetic principles, indicating that at equilibrium, the adsorption and desorption rates are equal, resulting in no net accumulation [36]. It is expressed as

$$\frac{1}{q_e} = \frac{1}{q_{max}} + \frac{1}{b q_{max} C_e} \quad (5)$$

where

- q_e (mg/g) represents the amount of adsorption at equilibrium;
- C_e (mg/L) denotes the equilibrium concentration of tetracycline remaining in the solution;
- q_{max} (mg/g) refers to the theoretical maximum adsorption capacity or monolayer saturation capacity;
- b (L/mg) is the Langmuir constant associated with adsorption equilibrium.

(b) Freundlich

This is a model that assumes that the distribution of the adsorption heat and the affinities for the heterogeneous surface are heterogeneous [36]. It is expressed as

$$lnq_e = lnK_f + \frac{1}{n} lnC_e \quad (6)$$

where

- q_e (mg/g) indicates the amount of adsorption at equilibrium;
- C_e mg/L) represents the equilibrium concentration of tetracycline remaining in the solution. (mg/L);
- K_f (mg·g^{-1}) is the Freundlich constant that represents the adsorption capacity;
- n is a dimensionless Freundlich constant that describes the desorption intensity.

2.12. Evaluation of Thermodynamic Parameters

The thermodynamic parameters were evaluated using these equations.

$$\Delta G^o = -RT\ InK_c \tag{7}$$

$$InK_c = \frac{\Delta S^o}{R} - \frac{\Delta H^o}{RT} \tag{8}$$

$$K_c = \frac{Cad}{C_e} \tag{9}$$

where

- C_e (mg/L) represents the equilibrium concentration of the tetracycline remaining in the solution;
- C_{ad} is the concentration of the metal in the adsorbent at equilibrium (mg/L);
- ΔG° is the Gibbs free energy (kJ/mol);
- ΔH° represents the standard enthalpy (kJ/mol);
- ΔS° is the standard entropy (J/mol/K).

The values of ΔG°, ΔH°, and ΔS° were determined using the plot of InK_c vs. 1/T(K).

3. Results

3.1. Characterisation of Composite Membrane

3.1.1. UV–Visible Spectroscopy

Figure 2 shows the full scan of tetracycline by a UV–Vis spectrophotometer. A UV–Vis scan of tetracycline was performed in the range of 300 to 800 nm at a scan rate of 3600 nm/min to determine the optimal wavelength for its maximum absorbance. We found 358 nm to be the best wavelength for the analysis of tetracyclines using a UV–Vis spectrophotometer, and it was used for the rest of the study. This peak (Figure 2) arises from the molecular structure of tetracycline, which includes conjugated systems, such as aromatic rings and double bonds, that absorb ultraviolet (UV) light. At this specific wavelength, the compound experiences electronic transitions, enabling accurate detection by spectrophotometry [37].

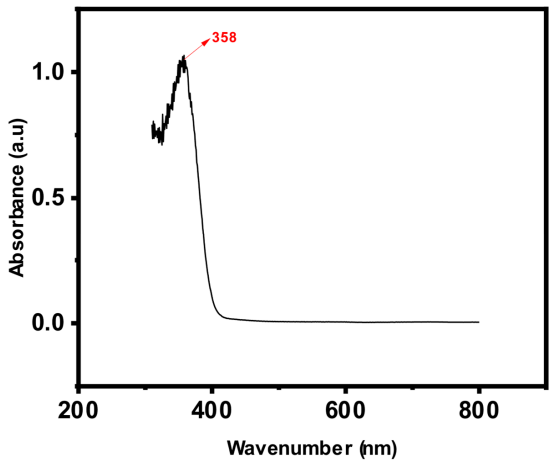

Figure 2. Full scan of tetracycline by UV–Vis spectrophotometer.

3.1.2. Fourier Transform Infrared (FTIR) Spectroscopy

The FTIR spectra of chitosan, FMWCNT–chitosan, and NMWCNT–chitosan nanocomposites are provided in Figure 3. All samples show broad and intense absorption bands in the 3200–3600 cm^{-1} range, attributed to overlapping stretching vibrations of -OH and $-NH_2$, which are characteristic of chitosan and consistent with its hydrophilic nature [38]. In the FMWCNT–chitosan and NMWCNT–chitosan spectra, these peaks are further broadened, indicating the incorporation of functionalised MWCNTs rich in hydroxyl group [39]. Distinct C–H stretching vibrations are observed in the region of 2923–2928 cm^{-1} (asymmetric) and 2840 cm^{-1} (symmetric), confirming the presence of alkyl groups in the core of chitosan composite. Peaks at 1650 cm^{-1} and 1554 cm^{-1} correspond to the C=O stretching of the amide groups ($–CONH_2$) and the bending of $-NH_2$, respectively, and are present in all spectra. Notably, the intensity of the peak at 1650 cm^{-1} in the FMWCNT–chitosan and NMWCNT–chitosan nanocomposites indicates a significant formation of new amide links. This phenomenon is attributed to the reaction between the COOH groups present in the MWCNTs and the $-NH_2$ groups of chitosan. Consequently, this interaction leads to the establishment of covalent bonds (-CONH-), which strengthen the composite structure. Furthermore, the bands in the 1430–1380 cm^{-1} region are attributed to C–N stretching vibrations, further supporting the presence of amide functionalities and effective integration of MWCNTs into the chitosan matrix [40].

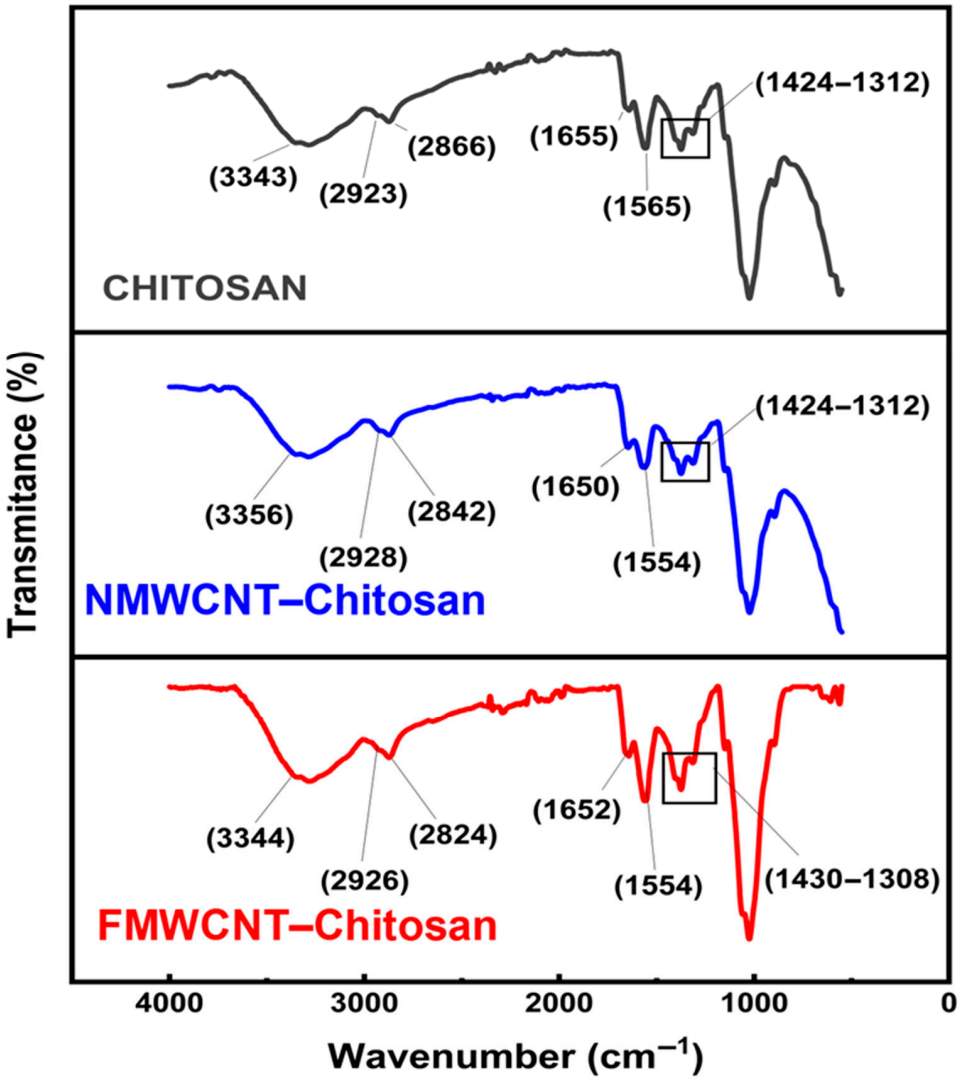

Figure 3. FTIR spectra of chitosan, NMWCNT–chitosan, and FMWCNT–chitosan.

3.1.3. Scanning Electron Microscopy and Energy-Dispersive Spectroscopy

Figure 4 shows SEM images of chitosan, FMWCNT–chitosan, and NMWCNT–chitosan nanocomposite materials. The surface of chitosan shows a rough and dense texture with a compact arrangement. Small granular formations are evident, suggesting a spongy surface. This morphology is advantageous for adsorption because it offers a greater number of sites for interactions with contaminants. The image in Figure 4b reveals fibrous structures, indicating the presence of carbon nanotube materials. These fibres appear to be more open and less tight, implying increased porosity. This fibrous network can improve the efficiency of adsorption by allowing tetracycline to penetrate the material's structure more effectively. The image in Figure 4c indicates that the surface exhibits rough and fibrous morphologies. The fibrous network contributes to mechanical stability and improved porosity, while the granular structure increases the available surface area. Together, these features enhance tetracycline adsorption through greater contact opportunities and molecular accessibility, as noted in the literature [20,41]. Additionally, the introduction of NMWCNTs to chitosan improved the surface of the chitosan structure, although not as highly as FMWCNTs.

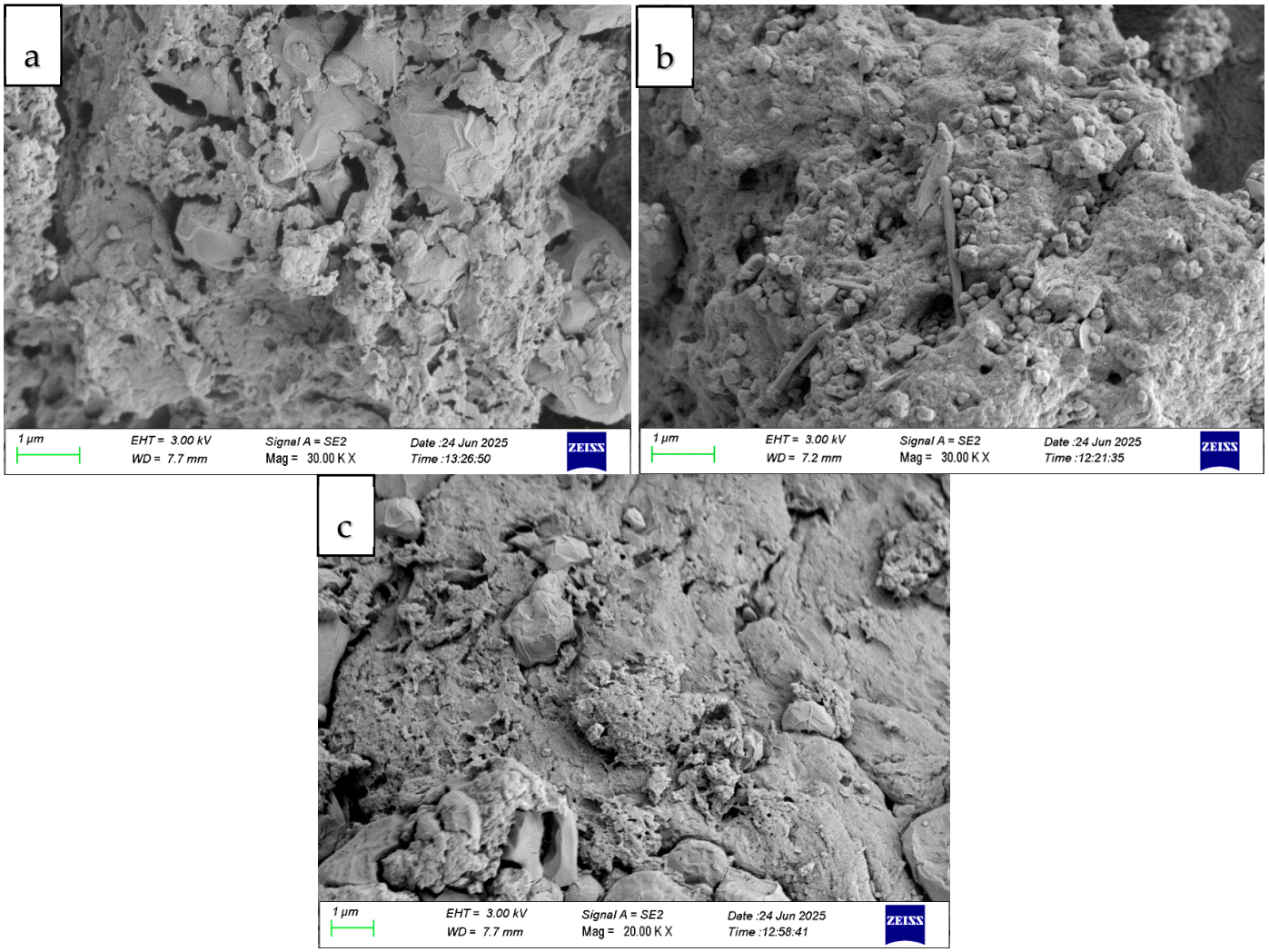

Figure 4. SEM images of (**a**) chitosan, (**b**) FMWCNT–chitosan, and (**c**) NMWCNT–chitosan nanocomposite materials.

3.1.4. X-Ray Diffraction (XRD)

Figure 5 shows the XRD patterns of chitosan, FMWCNT–chitosan, and NMWCNT–chitosan nanocomposite materials. The broad diffraction of chitosan with 2θ values of 20.0°

indicates the amorphous state of chitosan. Since only 1% of FMWCNTs and NMWCNTs were introduced to chitosan, the peaks of these composites only slightly broadened with few visible changes in structure. These chitosan nanocomposites exhibited a peak around 20°, associated with the (110) plane, suggesting that the crystalline properties are retained within the composite materials [20]. In the FMWCNT–chitosan composite, this peak becomes significantly broadened and reduced in intensity, suggesting that the incorporation of FMWCNTs disrupts the ordered crystalline structure of chitosan and increases the amorphous character of the material, potentially increasing the surface area [42]. This reduced crystal system likely facilitates improved adsorption by enhancing molecular diffusion and exposing more active sites.

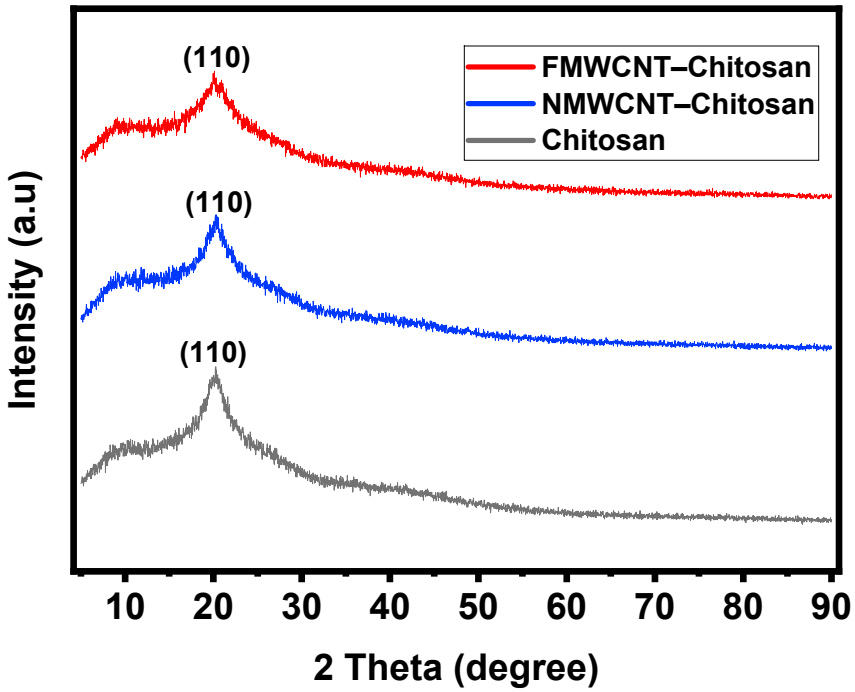

Figure 5. XRD patterns of chitosan, FMWCNT–chitosan, and NMWCNT–chitosan nanocomposite materials, showing the morphology of the structures.

Subsequently, the framework of MWCNTs on chitosan exhibits a strong impact on the properties of the chitosan composite. Although a lower percentage of MWCNTs were doped, MWCNT–chitosan grafting slightly affected the intensity and peak position of the carbon nanotube phase [43].

3.1.5. Thermogravimetric Analysis (TGA)

Figure 6 illustrates the thermal stability of the synthesised nanocomposites (chitosan, FMWCNT–chitosan, and NMWCNT–chitosan). All three materials exhibit similar thermal behaviour in the initial thermal analysis stages (0° to 300 °C). The nanocomposites underwent significant weight loss beginning around 200 °C, with a steep decline up to 400 °C, indicating their relatively low thermal stability and nearly complete decomposition by approximately 600 °C. This behaviour aligns with the known thermal degradation pattern of chitosan, which occurs in two stages: dehydration below 200 °C, followed by depolymerisation between 200 and 400 °C [44]. The NMWCNT–chitosan nanocomposite demonstrates enhanced thermal resistance, retaining more weight beyond 600 °C due to the stabilising effect of nitrogen doping, which strengthens interfacial interactions between chitosan and the nanotubes [45]. However, degradation continues beyond 600 °C, with maximum decomposition occurring at approximately 800 °C. In contrast, FMWCNT–chitosan exhibits

the highest thermal stability, maintaining significant residual weight even beyond 600 °C, with degradation extending up to 900 °C. This superior stability is attributed to the reinforcing effect of FMWCNTs, which form a robust network within the chitosan matrix [46]. The interfacial adhesion between the nanotubes and the polymer matrix is improved when the functional groups on FMWCNTs, such as -COOH and -OH, form hydrogen bonds with the hydroxyl (-OH) and amine (-NH_2) groups in chitosan. This improved interaction strengthens the composite structure, thereby increasing thermal resistance and reducing degradation [44]. Although nitrogen doping enhances π–π interactions, nitrogen groups like pyridinic N and graphitic N lack the strong hydrogen bonding and covalent linkages seen with oxygen-containing groups in FMWCNTs [47]. This difference likely contributes to the slightly lower adsorption performance.

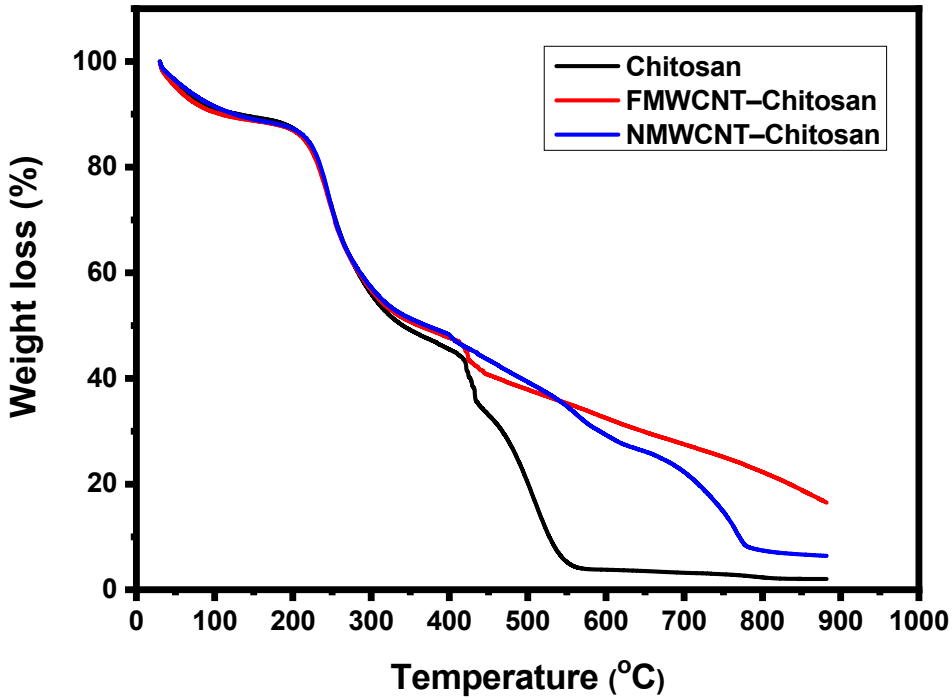

Figure 6. TGA curves of chitosan, FMWCNT–chitosan, and NMWCNT–chitosan nanocomposite materials.

3.1.6. BET Studies

The BET data for chitosan, FMWCNT–chitosan, and NMWCNT–chitosan nanocomposite materials are presented in Table 2. The BET data show that the chitosan had a lower surface area and pore volume; however, upon modification with either FMWCNTs or NMWCNTs, the surface area increased. Chitosan blending with FMWCNTs showed a greater increase in surface area (2.3882 m^2/g) compared to chitosan blending with N–doped MWCNTs (1.6836 m^2/g). It is suggested that the observed increase in the surface area of FMWCNT–chitosan resulted from improved interfacial interactions between the FMWCNTs and the surface of chitosan. The change in BET surface area is as follows: FMWCNT–chitosan > NMWCNT–chitosan > chitosan. The increase in surface area can be attributed to the formation of pores due to the incorporation of NMWCNTs, which is further enhanced by the addition of FMWCNTs to the chitosan compound as noted in the literature. The BET results correlate with the adsorption studies reported in Section 3.2 wherein the nanocomposite with the highest surface showed the highest adsorption of tetracycline in water samples.

Table 2. BET surface area and average pore volume of chitosan, FMWCNT–chitosan, and NMWCNT–chitosan nanocomposite materials.

Membrane	BET Surface Area (m^2/g)	Pore Volume (cm^3/g)
Chitosan	1.2823	0.00109
FMWCNT–chitosan	2.3882	0.004136
NMWCNT–chitosan	1.6836	0.00178

The adsorption capacities of the nanocomposites were evaluated using N_2 adsorption–desorption measurements. Figure 7 presents the nitrogen adsorption–desorption isotherms of chitosan, FMWCNT–chitosan, and NMWCNT–chitosan. Among these, FMWCNT–chitosan exhibited a distinctly higher nitrogen uptake, indicating enhanced porosity. According to the IUPAC classification, all the isotherms corresponded to Type IV profiles with H3 hysteresis loops, characteristic of mesoporous materials with slit-shaped pores and diameters ranging from 2 to 50 nm [48].

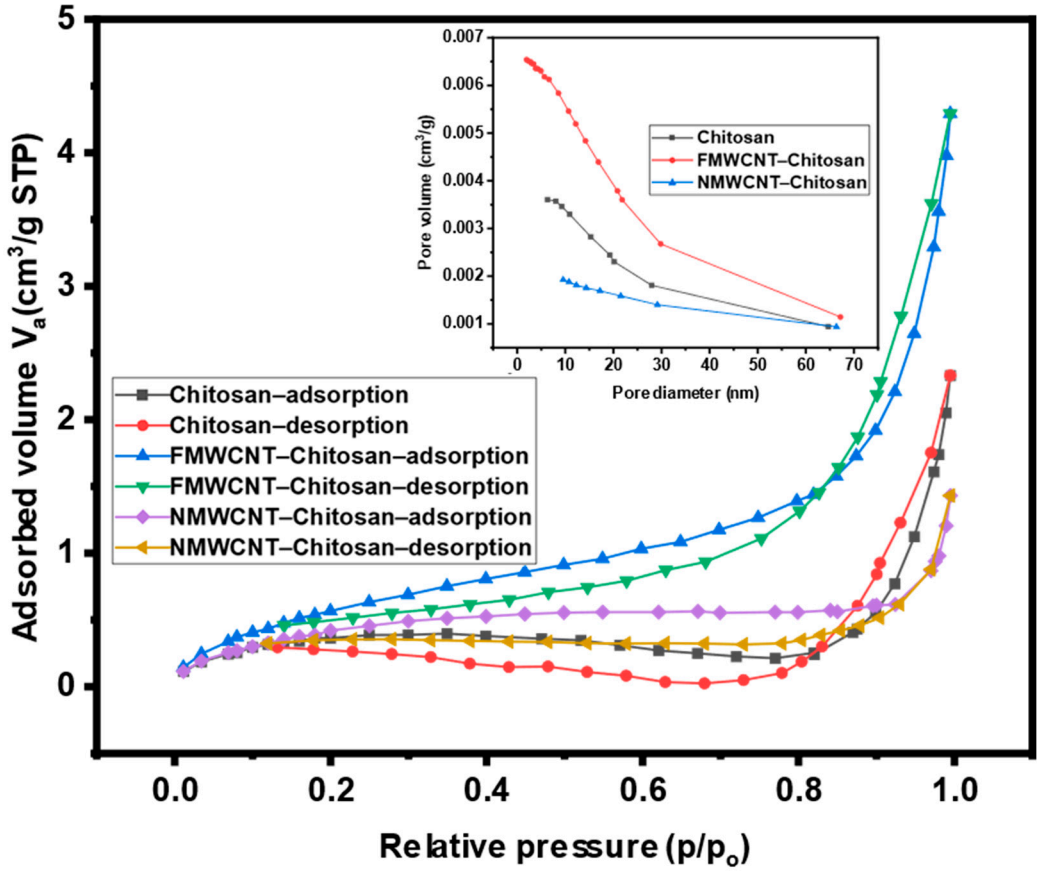

Figure 7. Nitrogen adsorption and desorption isotherms and BJH pore size distribution of chitosan, FMWCNT–chitosan, and NMWCNT–chitosan.

Also, Figure 7 (insert) includes pore size distribution curves obtained using the Barrett–Joyner–Halenda (BJH) method [49]. The mean pore diameters were found to be 20.19 nm for chitosan, 12.69 nm for FMWCNT–chitosan, and 22.66 nm for NMWCNT–chitosan. The results indicated that the addition of FMWCNTs showed the highest increase in pore volume, as the amount of N_2 adsorbed significantly increased. These results support the observed superior adsorption performance of FMWCNT–chitosan in tetracycline removal, which can be attributed to the increased surface area and improved accessibility of mesoporous sites.

3.2. Adsorption Studies

Several recent studies have demonstrated the importance of optimising process parameters to enhance the adsorption efficiency of multi-walled carbon nanotube (MWCNT)-based adsorbents for the removal of tetracycline. For example, Khazaie et al. [28] synthesised MWCNTs doped with aspartic acid (Asp) and polypyrrole (PPy), achieving a maximum adsorption capacity of 34.50 mg/g under optimised conditions: a dosage of 0.005 g adsorbent, pH 5, contact time 60 min, and 25 °C. The composite also retained a removal efficiency of more than 70% after seven reuse cycles, highlighting its operational stability. These findings reinforce the need for systematic optimisation when designing MWCNT-based adsorbents for practical applications.

3.2.1. Effect of pH

The effect of pH on tetracycline adsorption in chitosan, FMWCNT–chitosan, and NMWCNT–chitosan is depicted in Figure 8. pH plays a crucial role in determining how tetracycline interacts with adsorbents by affecting the ionisation state of antibiotics, the surface charge of the adsorbents, and the various mechanisms involved in adsorption [50]. As shown in Figure 8, the percentage removal of tetracycline increases with rising pH; this is because, at higher pH levels, tetracycline becomes less protonated, reducing its positive charge and enhancing its interaction with the adsorbent. The highest adsorption efficiency was observed at pH 6, which lies near the neutral region where tetracycline predominantly exists in a neutral or slightly anionic form. Under these conditions, adsorption is maximised due to minimal electrostatic repulsion between the adsorbate and the adsorbent [51,52]. Furthermore, at pH 6, chitosan becomes more hydrophobic, and the hydrophobicity of incorporated FMWCNTs and NMWCNTs further enhances their interaction with tetracycline through hydrophobic forces. As pH increases beyond 6, tetracycline becomes more negatively charged due to deprotonation of its functional groups [53,54]. Simultaneously, the surface of the adsorbents also becomes deprotonated and becomes negatively charged due to deprotonation of –OH and –COOH groups, as supported by FTIR shifts, resulting in a negatively charged surface. This leads to electrostatic repulsion between the negatively charged adsorbate and the adsorbent, which contributes to the observed decrease in the adsorption efficiency at higher pH values.

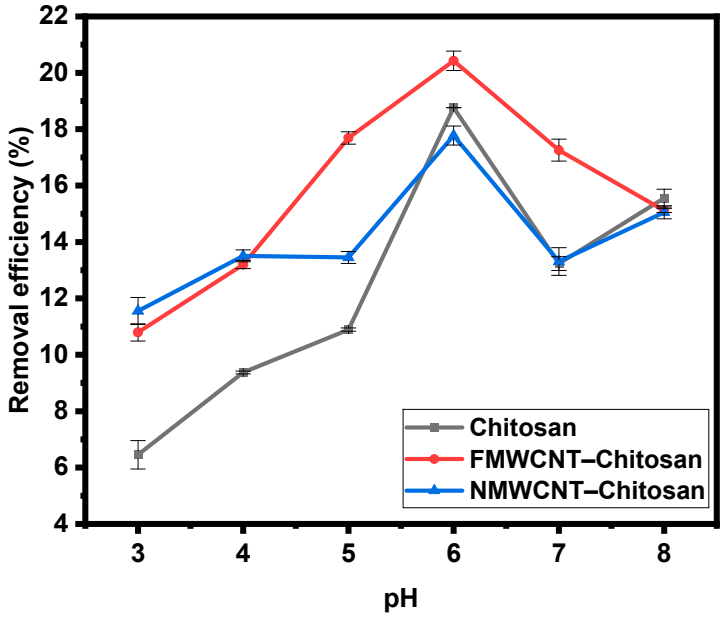

Figure 8. Effect of pH on the adsorption of tetracycline in chitosan, FMWCNT–chitosan, and NMWCNT–chitosan.

3.2.2. Effect of Dosage

A crucial element in creating an effective adsorption system is the amount of adsorbent that is used, and this plays a crucial role in optimising the adsorption process. As shown in Figure 9, the percentage of adsorption increased significantly when the dose increased from 1 g/L to 2 g/L, due to the greater surface area and availability of active sites. However, an additional increase in dose led to a gradual decline in adsorption efficiency, likely due to particle agglomeration and overlap of adsorption sites [55]. Since the initial concentration of tetracycline in the simulated wastewater was consistent in all adsorption experiments, an excessive amount of tetracycline remained in the solution when the dosage of the adsorbent was lower [37]. With these lower dosages, the free adsorption sites on the surface of the chitosan nanocomposite were able to interact quickly with tetracycline, rapidly reaching saturation and resulting in a high adsorption capacity as reported in the literature [10,56]. Therefore, the adsorbent dosage for the rest of the study was 2 g/L. The figure clearly demonstrates the superior performance of FMWCNT–chitosan, which exhibited the highest removal efficiency despite all composites being tested at the same dosage. This enhanced adsorption can be attributed to its larger surface area, as confirmed by BET analysis. FMWCNT–chitosan exhibited a surface area of 2.3882 m^2/g, followed by NMWCNT–chitosan (1.6836 m^2/g) and chitosan (1.2823 m^2/g).

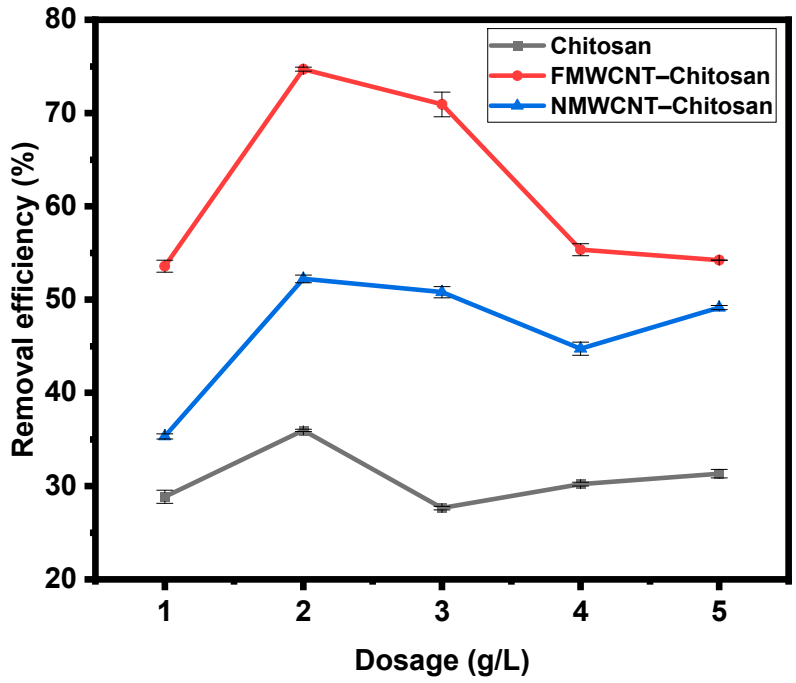

Figure 9. Effect of dosage on the adsorption of tetracycline by chitosan, FMWCNT–chitosan, and NMWCNT–chitosan.

3.2.3. Effect of Concentration

The level of tetracycline in a solution can greatly influence multiple aspects of the adsorption process and the effectiveness of treatment. Figure 10 shows the effect of concentration studied during the adsorption of tetracycline by chitosan, FMWCNT–chitosan, and NMWCNT–chitosan nanocomposites. As shown in Figure 10, an increase in the initial concentration of tetracycline led to a reduction in its removal efficiency. At lower concentrations, there are often many available adsorption sites, resulting in higher removal rates. However, once saturation occurs, further increases in concentration may not substantially improve adsorption. These results indicate that optimal adsorption occurs at lower con-

centrations of tetracycline, in agreement with previous studies [57]. The chosen optimum concentration was 10 ppm.

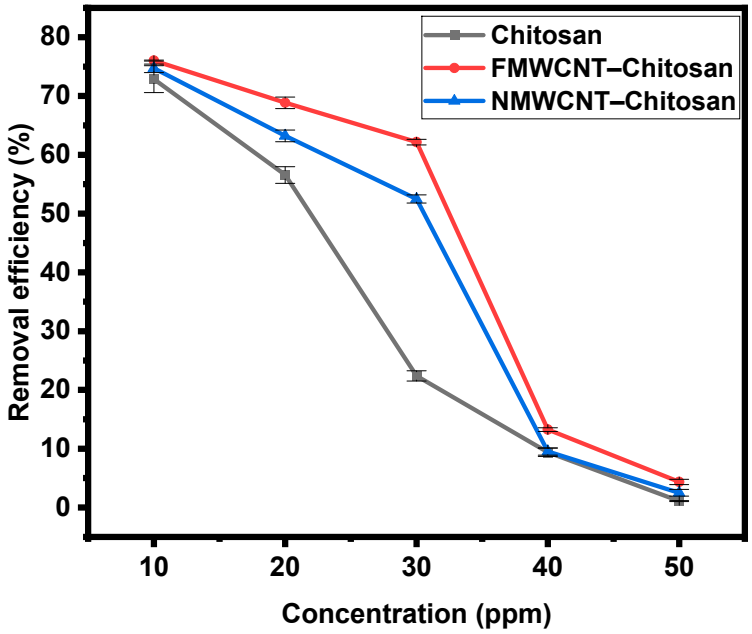

Figure 10. Effect of concentration on the adsorption of tetracycline by chitosan, FMWCNT–chitosan, and NMWCNT–chitosan.

3.2.4. Effect of Contact Time

Contact time plays a critical role in the adsorption process, influencing both the efficiency and kinetics of tetracycline removal. Figure 11 shows the effect of time studied during the adsorption of tetracycline by chitosan, FMWCNT–chitosan, and NMWCNT–chitosan nanocomposites. As shown in Figure 11, a rapid adsorption phase occurred within the first 20 min, followed by a gradual plateau, with equilibrium reached at approximately 30 min. This initial rapid uptake is attributed to the large number of available active sites on the nanocomposite surface, particularly in the FMWCNT–chitosan sample, which possesses a higher surface area, as revealed by BET analysis. The porous, semi-crystalline structure observed in SEM and XRD further facilitates fast diffusion and interaction of tetracycline molecules with the adsorbent. After 30 min, the adsorption rate slowed significantly due to site saturation, consistent with previous findings [11,58]. Equilibrium adsorption was reached at 30 min.

3.3. Reusability Studies

Reusable adsorbents reduce the need for frequent replacement, thereby reducing operational costs, especially in large-scale applications. This is particularly beneficial in large-scale applications where the upfront investment in high-quality adsorbents can be considerable. Figure 12 shows the adsorption–desorption results (five cycles) of chitosan, FMWCNT–chitosan and NMWCNT–chitosan. The adsorption capacity decreased from 73% to 70% for chitosan, from 80% to 77% for NMWCNT–chitosan, and from 87% to 85% for FMWCNT–chitosan between the first and fifth cycles, as noted in the literature [43]. The highest efficiency and stability in degradation across multiple cycles are demonstrated, and NMWCNT–chitosan closely follows. In comparison, pure chitosan shows satisfactory performance, although its efficiency is lower.

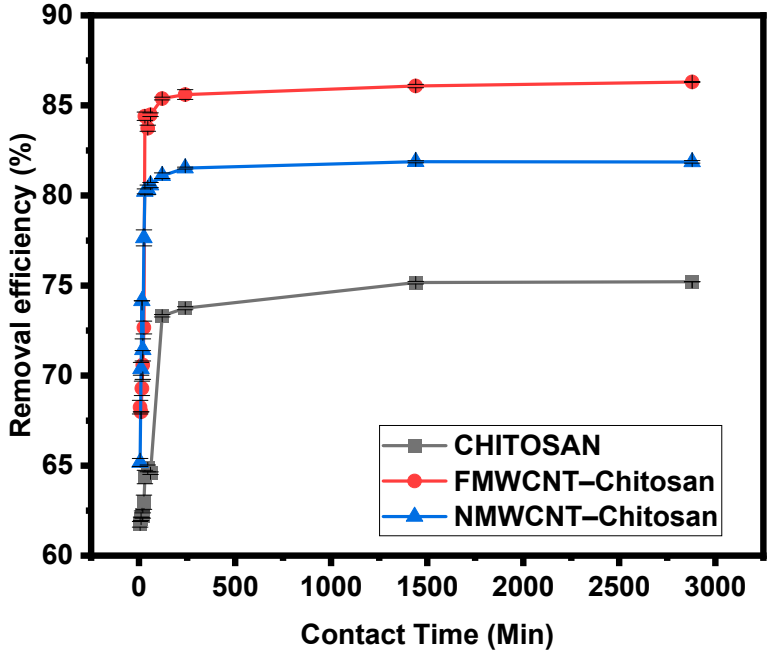

Figure 11. Effect of contact time on the adsorption of tetracycline by chitosan, FMWCNT–chitosan, and NMWCNT–chitosan.

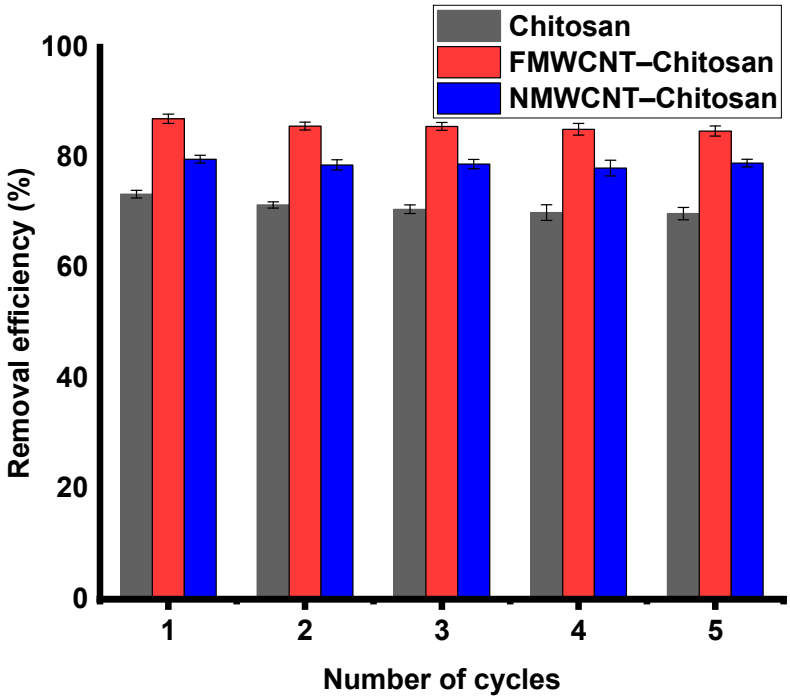

Figure 12. Reusability of chitosan, FMWCNT–chitosan, and NMWCNT–chitosan in the adsorption of tetracycline.

3.4. Effect of Ionic Strength

Figure 13 shows the effect of ionic strength studied during the adsorption of tetracycline by FMWCNT–chitosan nanocomposites. The results showed that the FMWCNT–chitosan nanocomposite retained a high removal efficiency of 82%, even in the presence of these common background ions. This represents a slight decrease of only 3% compared to the ion-free solution, as represented in Figure 13. The minor reduction in performance is probably due to limited competition between the coexisting anions and tetracycline

molecules for adsorption sites, indicating that the composite is effective under realistic water treatment conditions [59].

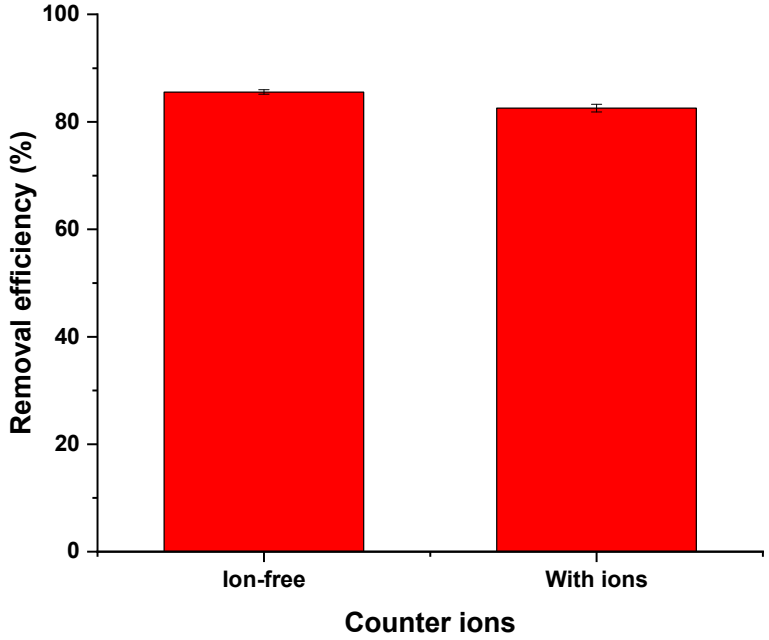

Figure 13. Effect of ionic strength on the adsorption of tetracycline by a FMWCNT–chitosan nanocomposite at pH 6, 25 °C, and an adsorbent dose of 2 g/L. The solution contained 10 ppm tetracycline and background ions (SO_4^{2-} 50 mg/L, NO_3^- 5 mg/L, Cl^- 60 mg/L).

3.5. Effect of a Binary System

In real water samples, multiple pharmaceuticals and contaminants often coexist, potentially affecting the removal of each other. Figure 14 shows the effect of ionic strength studied during the adsorption of tetracycline by FMWCNT–chitosan nanocomposites. The results showed that in the binary system, the removal efficiency of tetracycline decreased to 70%, representing a notable reduction of 15% compared to the single component system, as represented in Figure 14. This decline is attributed to the competitive adsorption between tetracycline and tylosin, where both pharmaceuticals compete for available active sites on the FMWCNT–chitosan surface, thereby reducing the number of sites accessible for tetracycline uptake as noted in the literature [60,61].

3.6. Adsorption Kinetics

The adsorbent's kinetic behaviour was investigated using pseudo-first- and pseudo-second-order models to help identify the type of sorption occurring. Figure 15a,b show the linearised equations and graphs for the pseudo-first-order and pseudo-second-order adsorption models for tetracycline, respectively. Table 3 shows the kinetic parameters for the adsorption of tetracycline by chitosan, FMWCNT–chitosan and NMWCNT–chitosan. The data indicate that the adsorption kinetics align more closely with a pseudo-second-order reaction, as evidenced by the higher R^2 values (0.9992, 0.9455, and 0.9844) compared to the pseudo-first-order model (0.9733, 0.7823, and 0.9285). The experimental q_e values were in good agreement with those predicted by the pseudo-second-order model, particularly for NMWCNT–chitosan. The pseudo-first-order model, on the contrary, showed poor R^2 values and substantial discrepancies between the predicted and experimental q_e values, suggesting that it does not adequately describe the system. The superior performance of FMWCNT–chitosan is also reflected in the relatively high rate constant (k_2 = 0.132 g/mg·min) and strong fit (R^2 = 0.9844), although its modelled q_e slightly underestimated the experimental value, possibly due to additional adsorption contributions not captured by the model. The

higher performance of FMWCNT–chitosan is attributed to its numerous surface functional groups, as verified by FTIR analysis, and a highly porous structure, as seen in SEM images. A decreased crystallinity was indicated by XRD patterns, along with the large surface area measured by BET. This suggests that chemisorption, characterised by stronger interactions between the adsorbate and the adsorbent, probably drives the process [62,63], rather than the weaker physisorption interactions typically linked with pseudo-first-order kinetics.

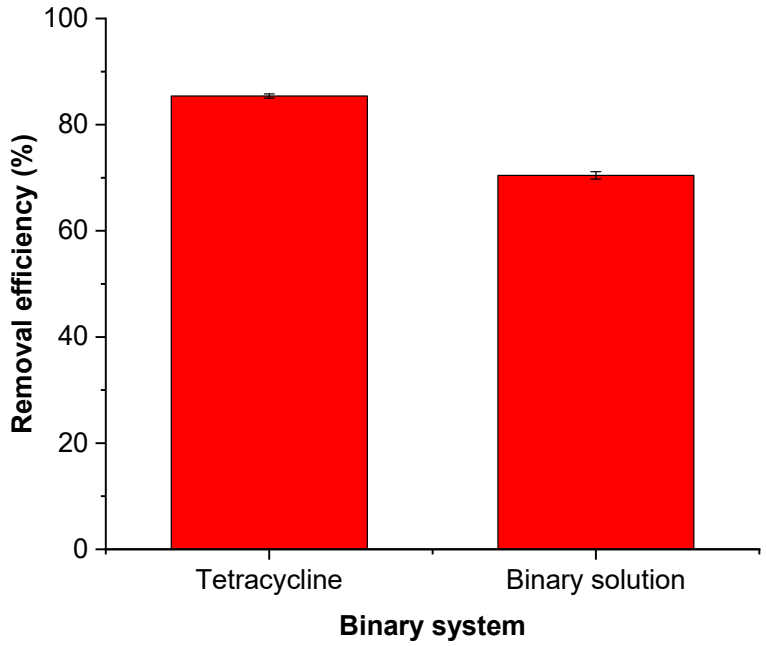

Figure 14. Effect of a binary pharmaceutical system on the adsorption efficiency of tetracycline using a FMWCNT–chitosan nanocomposite. Adsorption conditions: pH 6, adsorbent dosage 2 g/L, contact time 30 min, and temperature 25 °C. In the binary solution (10 ppm).

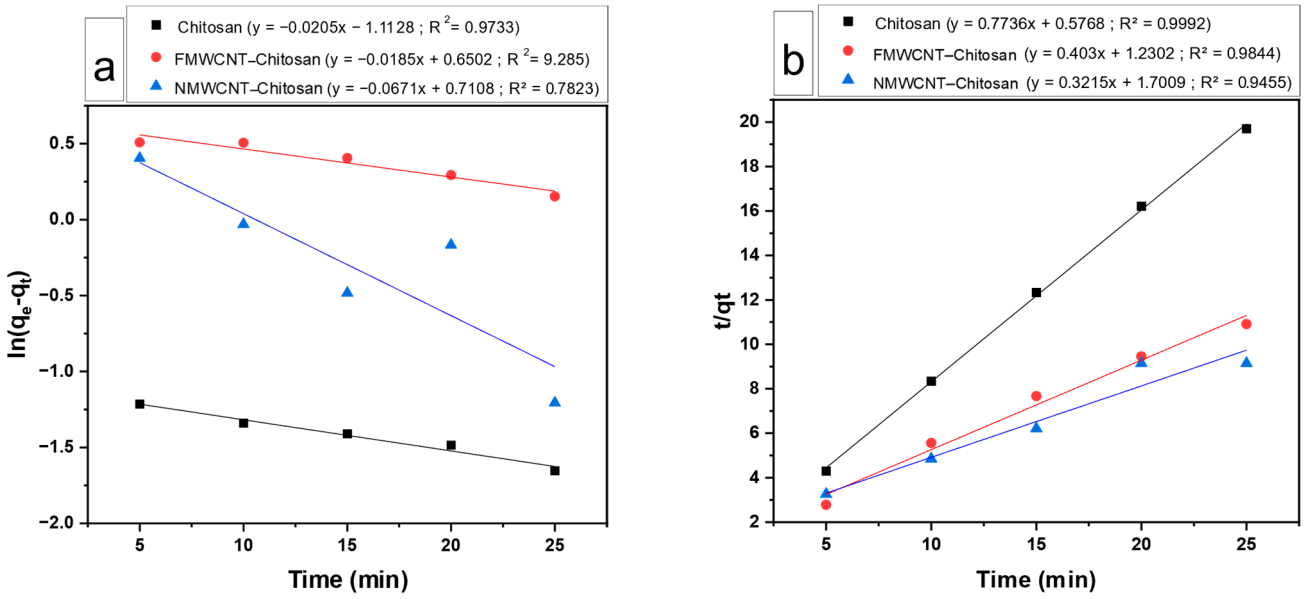

Figure 15. Kinetic behaviour of chitosan, FMWCNT–chitosan, and NMWCNT–chitosan using (**a**) pseudo-first-order and (**b**) pseudo-second-order kinetics.

Table 3. Kinetic parameters for the adsorption of tetracycline by chitosan, FMWCNT–chitosan, and NMWCNT–chitosan.

Membrane	Experimental Q_e ($mg \cdot g^{-1}$)	Pseudo-First-Order Kinetic Model			Pseudo-Second-Order Kinetic Model		
		K_1	Q_e ($mg \cdot g^{-1}$)	R^2	K_2	Q_e ($mg \cdot g^{-1}$)	R^2
Chitosan	2.46	0.0205	0.324	0.9733	1.04	1.29	0.9992
FMWCNT–chitosan	3.46	0.0671	2.04	0.9285	0.132	2.48	0.9844
NMWCNT–chitosan	3.03	0.0185	1.92	0.7823	0.603	3.12	0.9455

3.7. Adsorption Isotherm

The linearised data from the Langmuir and Freundlich isotherms used to adsorb the tetracycline composite membranes are shown in Figure 16. The adsorption isotherm offers valuable insights into the mechanisms underlying the adsorption process. Table 4 lists the simulation parameters of the model for each model. R^2 values indicate that the adsorption processes of all composite membranes closely follow the Langmuir model. This suggests that adsorption likely occurs on a homogeneous surface, with a finite number of identical sites, and is limited to monolayer coverage on membrane surfaces [64]. The maximum tetracycline adsorption capacity of the chitosan nanomaterial, determined by fitting the nonlinear curve, was 263.16, 86.96, and 149.25 $mg \cdot g^{-1}$ of adsorbent for chitosan NMWCNT–chitosan, and FMWCNT–chitosan, respectively. The value of RL for all adsorbents falls in this range of $0 < RL < 1$. The adsorption process is considered favourable, which means that the adsorbent has a strong attraction for the adsorbate, so as the adsorbate concentration increases, the quantity of adsorbed also increases, as noted elsewhere [65,66].

Table 4. Parameters of Langmuir and Freundlich isotherms for tetracycline adsorption by chitosan, FMWCNT–chitosan, and NMWCNT–chitosan.

Membrane	Langmuir Model				Freundlich Model		
	R_L	q_m (mg/g)	b (L/mg)	R^2	K_f (mg/g)	*n*	R^2
Chitosan	0.9812	86.96	0.001879	0.9991	0.5731	1.066	0.9918
FMWCNT–chitosan	0.9683	263.16	0.003278	0.9978	0.6701	1.514	0.9726
NMWCNT–chitosan	0.947	149.25	0.005581	0.9963	0.6384	1.378	0.9779

3.8. Thermodynamic Analysis

Thermodynamic analysis is used to examine the spontaneity, ability, and heat of tetracycline adsorption and the values of the thermodynamic parameters are key indicators of process applicability [67]. Thermodynamic characteristics under ideal circumstances were determined using the amounts of tetracycline adsorbed onto the adsorbent surface at various temperatures (25, 30, 35, and 40 °C) and plotted in Figure 17. Based on the slopes and intercept of the Van't Hoff plot, as illustrated in Figure 17, the Gibbs free energy (ΔG°), standard enthalpy (ΔH°), and standard entropy (ΔS°) for chitosan, FMWCNT–chitosan, and NMWCNT–chitosan composite membranes were calculated and are summarised in Table 5.

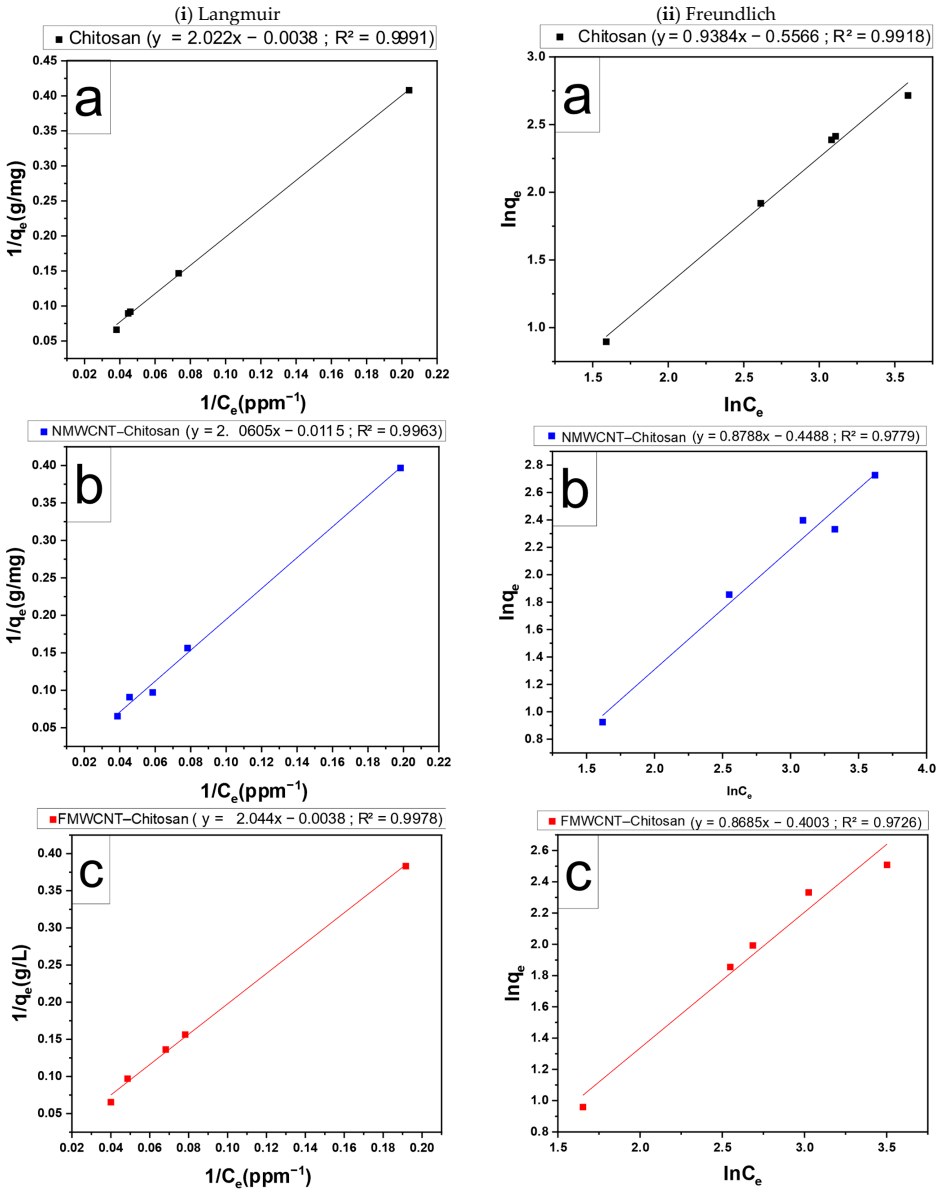

Figure 16. (**i**) Langmuir isotherm adsorption and (**ii**) Freundlich isotherm of (**a**) chitosan, (**b**) NMWCNT–chitosan, and (**c**) FMWCNT–chitosan on the adsorption of tetracycline.

The negative ΔG° values observed for FMWCNT–chitosan indicate that adsorption is a spontaneous and favourable process, as reported elsewhere [68,69]. However, NMWCNT–chitosan was favourable only at room temperature (25 °C). More negative ΔG° values indicate a stronger driving force for adsorption. Conversely, increasing ΔG° with rising temperature suggests reduced adsorption efficiency at elevated temperature; a comparable effect was observed by Uzun & Güzel, 2004 [64]. Negative ΔH° values confirm the exothermic nature of the adsorption process while the negative ΔS° value suggests a decrease in randomness at the solid–solution interface during the adsorption of tetracycline [70]. Moreover, the negative ΔH° and ΔS° values imply that enthalpy has a greater contribution than entropy in generating the negative ΔG° values, and a similar behaviour of thermodynamic parameter values was reported in the literature [69,70].

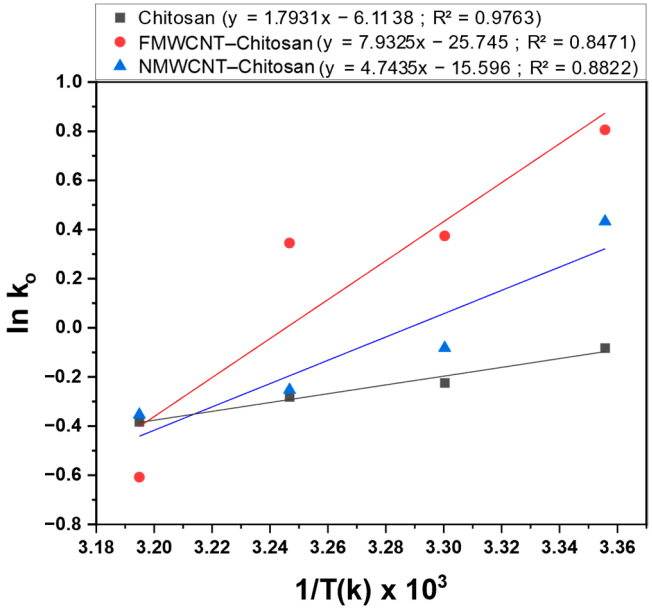

Figure 17. Van't Hoff plot for the adsorption of tetracycline by chitosan for tetracycline adsorption by chitosan, FMWCNT–chitosan, and NMWCNT–chitosan.

Table 5. Value of thermodynamic parameters for the tetracycline adsorption by chitosan for tetracycline adsorption by chitosan, FMWCNT–chitosan, and NMWCNT–chitosan.

Membrane	**Thermodynamic Parameters**			
	Temperature (K)	**ΔG° (kJ·mol^{-1})**	**H (kJ·mol^{-1})**	**S (J·mol·K^{-1})**
Chitosan	298	0.203	−0.0149	−50.83
	303	0.564		
	308	0.720		
	313	0.996		
FMWCNT–chitosan	298	−1.996	−0.0660	−214.04
	303	−0.941		
	308	−0.882		
	313	1.582		
NMWCNT–chitosan	298	−1.072	−0.0394	−129.67
	303	0.206		
	308	0.646		
	313	0.920		

4. Conclusions

This study successfully explored the synthesis and application of chitosan-based nanocomposites for the efficient removal of tetracycline from aqueous solutions. Incorporating functionalised and nitrogen-doped multi-walled carbon nanotubes (FMWCNTs and NMWCNTs) significantly enhanced the structural and functional characteristics of chitosan. Characterisation using FTIR, SEM, XRD, BET, and TGA successfully confirmed the synthesises of the nanocomposites, while BET analysis showed the surface characteristics of the nanocomposites. The resulting nanocomposites demonstrated notable improvements in adsorption efficiency, thermal stability, mechanical strength, and reusability. The FMWCNT–chitosan composite exhibited excellent adsorption properties in the presence of counter ions (82%) and in a binary system (70%). Among the materials tested, the FMWCNT–chitosan composite exhibited the best performance, achieving a rapid adsorption rate, a maximum adsorption capacity of 263.16 mg/g, and a removal efficiency of 85%. This was achieved with a pH of 6, 2 g/L adsorbent dosage, 10 ppm concentration,

30 min contact time, and 25 °C. Kinetic studies indicated that the adsorption process followed a pseudo-second-order model for all nanocomposites, while isotherm analysis showed good agreement with the Langmuir model, suggesting monolayer adsorption on a homogeneous surface. Thermodynamic evaluations further confirmed that adsorption was spontaneous and exothermic, and FMWCNT–chitosan showed the most favourable thermodynamic behaviour.

The adsorption experiments in this study were conducted under controlled laboratory conditions using synthetic tetracycline solutions, which presents a key limitation. The effectiveness of the chitosan-based nanocomposites in treating complex real-world wastewater containing a wide array of organic and inorganic co-contaminants remains to be evaluated. Future research should focus on assessing the performance of these materials in actual wastewater matrices to better simulate practical applications. Additionally, integrating photocatalytic components into the nanocomposites may offer a dual-function approach, combining adsorption with photodegradation. This could significantly enhance the removal efficiency of pharmaceutical pollutants while reducing the risk of secondary contamination due to adsorbent saturation or desorption.

Author Contributions: Conceptualization, L.E.M.; formal analysis, L.E.M.; funding acquisition, L.E.M.; investigation, M.S.K.; methodology, M.S.K. and L.E.M.; project administration, L.E.M. and C.P.M.; resources, L.E.M.; supervision, L.E.M. and C.P.M.; validation, L.E.M. and C.P.M.; writing—original draft, M.S.K.; writing—review and editing, M.S.K., L.E.M. and C.P.M. All authors have read and agreed to the published version of the manuscript.

Funding: This research was funded by the National Research Foundation Thuthuka, funding number: TTK2203311375.

Data Availability Statement: Data are contained within this article.

Acknowledgments: We would like to acknowledge The University of Limpopo Department of Chemistry for the opportunity to conduct the research.

Conflicts of Interest: The authors declare that they have no conflicts of interest.

References

1. Edokpayi, J.N.; Rogawski, E.T.; Kahler, D.M.; Hill, C.L.; Reynolds, C.; Nyathi, E.; Smith, J.A.; Odiyo, J.O.; Samie, A.; Bessong, P.; et al. Challenges to Sustainable Safe Drinking Water: A Case Study Ofwater Quality and Use across Seasons in Rural Communities in Limpopo Province, South Africa. *Water* **2018**, *10*, 159. [CrossRef]
2. Kümmerer, K. The Presence of Pharmaceuticals in the Environment Due to Human Use—Present Knowledge and Future Challenges. *J. Environ. Manage.* **2009**, *90*, 2354–2366. [CrossRef] [PubMed]
3. Kaczorowska, M.A.; Bożejewicz, D. The Application of Chitosan-Based Adsorbents for the Removal of Hazardous Pollutants from Aqueous Solutions—A Review. *Sustain* **2024**, *16*, 2615. [CrossRef]
4. Munwana, A.; Macevele, L.E. Diclofenac Sodium Removal from Water Samples Using Chitosan Nanocomposites Modified with Multi-Walled Carbon Nanotubes. *Dig. J. Nanomater. Biostructures* **2025**, *20*, 227–238. [CrossRef]
5. de Aquino, S.F.; Brandt, E.M.F.; Bottrel, S.E.C.; Gomes, F.B.R.; Silva, S.d.Q. Occurrence of Pharmaceuticals and Endocrine Disrupting Compounds in Brazilian Water and the Risks They May Represent to Human Health. *Int. J. Environ. Res. Public Health* **2021**, *18*, 11765. [CrossRef]
6. Arumugam, A.; Lee, K.E.; Ng, P.Y.; Shamsuddin, A.S.; Zulkifli, A.; Goh, T.L. Pharmaceuticals as Emerging Pollutants: Implications for Water Resource Management in Malaysia. *Emerg. Contam.* **2025**, *11*, 100470. [CrossRef]
7. Scott, T.M.; Phillips, P.J.; Kolpin, D.W.; Colella, K.M.; Furlong, E.T.; Foreman, W.T.; Gray, J.L. Pharmaceutical Manufacturing Facility Discharges Can Substantially Increase the Pharmaceutical Load to U.S. Wastewaters. *Sci. Total Environ.* **2018**, *636*, 69–79. [CrossRef]
8. Mathers, J.J.; Flick, S.C.; Cox, L.A. Longer-Duration Uses of Tetracyclines and Penicillins in U.S. Food-Producing Animals: Indications and Microbiologic Effects. *Environ. Int.* **2011**, *37*, 991–1004. [CrossRef]

9. Karimi-Maleh, H.; Ayati, A.; Davoodi, R.; Tanhaei, B.; Karimi, F.; Malekmohammadi, S.; Orooji, Y.; Fu, L.; Sillanpää, M. Recent Advances in Using of Chitosan-Based Adsorbents for Removal of Pharmaceutical Contaminants: A Review. *J. Clean. Prod.* **2021**, *291*, 125880. [CrossRef]
10. Erdem, S.; Öztekin, M.; Sağ Açıkel, Y. Investigation of Tetracycline Removal from Aqueous Solutions Using Halloysite/Chitosan Nanocomposites and Halloysite Nanotubes/Alginate Hydrogel Beads. *Environ. Nanotechnol. Monit. Manag.* **2021**, *16*, 100576. [CrossRef]
11. Guo, X.; Wu, Z.; Wang, Z.; Lin, F.; Li, P.; Liu, J. Preparation of Chitosan-Modified Bentonite and Its Adsorption Performance on Tetracycline. *ACS Omega* **2023**, *8*, 19455–19463. [CrossRef]
12. Bhatt, P.; Joshi, S.; Urper Bayram, G.M.; Khati, P.; Simsek, H. Developments and Application of Chitosan-Based Adsorbents for Wastewater Treatments. *Environ. Res.* **2023**, *226*, 115530. [CrossRef]
13. Wang, H.; Yang, J.; Zhang, H.; Zhao, J.; Liu, H.; Wang, J.; Li, G.; Liang, H. Membrane-Based Technology in Water and Resources Recovery from the Perspective of Water Social Circulation: A Review. *Sci. Total Environ.* **2024**, *908*, 168277. [CrossRef]
14. Awual, M.R.; Khraisheh, M.; Alharthi, N.H.; Luqman, M.; Islam, A.; Rezaul Karim, M.; Rahman, M.M.; Khaleque, M.A. Efficient Detection and Adsorption of Cadmium(II) Ions Using Innovative Nano-Composite Materials. *Chem. Eng. J.* **2018**, *343*, 118–127. [CrossRef]
15. Gkika, D.A.; Mitropoulos, A.C.; Kokkinos, P.; Lambropoulou, D.A.; Kalavrouziotis, I.K.; Bikiaris, D.N.; Kyzas, G.Z. Modified Chitosan Adsorbents in Pharmaceutical Simulated Wastewaters: A Review of the Last Updates. *Carbohydr. Polym. Technol. Appl.* **2023**, *5*, 100313. [CrossRef]
16. Anupam, K.; Dutta, S.; Bhattacharjee, C.; Datta, S. Adsorptive Removal of Chromium (VI) from Aqueous Solution over Powdered Activated Carbon: Optimisation through Response Surface Methodology. *Chem. Eng. J.* **2011**, *173*, 135–143. [CrossRef]
17. Khumalo, S.M.; Bakare, B.F.; Rathilal, S.; Khodakarami, M.; Honaker, R. Single and Multicomponent Adsorption of Amoxicillin, Ciprofloxacin, and Sulfamethoxazole on Chitosan-Carbon Nanotubes Hydrogel Beads from Aqueous Solutions: Kinetics, Isotherms, and Thermodynamic Parameters. *J. Hazard. Mater. Adv.* **2024**, *912*, 169519. [CrossRef]
18. Petrović, M.; Gonzalez, S.; Barceló, D. Analysis and Removal of Emerging Contaminants in Wastewater and Drinking Water. *TrAC —Trends Anal. Chem.* **2003**, *22*, 685–696. [CrossRef]
19. Omran, K.A.; El-Aassar, M.R.; Ibrahim, O.M.; Sharaewy, S.A.; Khalifa, R.E.; Mohamed, F.M. Chitosan/Alginate Nanocomposites Containing Magnetic Nanoparticles and Multi-Wall Carbon Nanotubes for Efficient Iron Sorption. *Desalin. Water Treat.* **2024**, *317*, 100294. [CrossRef]
20. Chandra Dey, S.; Al-Amin, M.; Ur Rashid, T.; Zakir Sultan, M.; Ashaduzzaman, M.; Sarker, M.; Md Shamsuddin, S. Preparation, Characterization and Performance Evaluation of Chitosan As an Adsorbent for Remazol Red. *Int. J. Latest Res. Eng. Technol.* **2016**, *2*, 52–62.
21. Larrude, D.G.; Maia Da Costa, M.E.H.; Freire, F.L. Synthesis and Characterization of Silver Nanoparticle-Multiwalled Carbon Nanotube Composites. *J. Nanomater.* **2014**, *2014*, 654068. [CrossRef]
22. Rananga, L.E.; Magadzu, T. Comparative Studies of Silver Doped Carbon Nanotubes and β-Cyclodextrin for Water Disinfection. *Dig. J. Nanomater. Biostructures* **2015**, *10*, 831–836.
23. Gonçalves, L.P.L.; Meledina, M.; Meledin, A.; Petrovykh, D.Y.; Sousa, J.P.S.; Soares, O.S.G.P.; Kolen'ko, Y.V.; Pereira, M.F.R. Understanding the Importance of N−doping for CNT-Supported Ni Catalysts for CO_2 Methanation. *Carbon* **2022**, *195*, 35–43. [CrossRef]
24. Babel, S.; Kurniawan, T.A. Low-Cost Adsorbents for Heavy Metals Uptake from Contaminated Water: A Review. *J. Hazard. Mater.* **2003**, *97*, 219–243. [CrossRef]
25. Słomkiewicz, P.M.; Dołęgowska, S.; Wideł, D.; Piekacz, K. Adsorption Isotherms for Tetracycline Removal from Water Using Carbon-Mineral Composites Determined by Inverse Liquid Chromatography. *Desalin. Water Treat.* **2025**, *322*, 7–12. [CrossRef]
26. Yu, H.; Gao, L.; Zhang, X.; Zhang, S.; Chi, W.; Zhang, L.; Li, J.; Tian, Y.; Cai, H.; Zhang, Y. Enhanced Removal of Tetracycline from Water Using MgO-Modified g-C_3N_4 Composite: Synthesis Optimization and Mechanism Investigation. *J. Water Process Eng.* **2025**, *71*, 107176. [CrossRef]
27. Sağlam, S.; Türk, F.N.; Arslanoğlu, H. Tetracycline (TC) Removal from Wastewater with Activated Carbon (AC) Obtained from Waste Grape Marc: Activated Carbon Characterization and Adsorption Mechanism. *Environ. Sci. Pollut. Res.* **2024**, *31*, 33904–33923. [CrossRef] [PubMed]
28. Khazaie, A.; Kia, H.; Moniri, E.; Hassani, A.H.; Miralinaghi, M. Adsorption Modeling of Tetracycline Removal by Multi-Walled Carbon Nanotube Functionalized with Aspartic Acid and Poly-Pyrrole Using Bayesian Optimized Artificial Neural Network. *J. Taiwan Inst. Chem. Eng.* **2023**, *144*, 104743. [CrossRef]
29. Chang, J.; Shen, Z.; Hu, X.; Schulman, E.; Cui, C.; Guo, Q.; Tian, H. Adsorption of Tetracycline by Shrimp Shell Waste from Aqueous Solutions: Adsorption Isotherm, Kinetics Modeling, and Mechanism. *ACS Omega* **2020**, *5*, 3467–3477. [CrossRef]
30. Hamoudi, S.A.; Hamdi, B.; Brendlé, J. Tetracycline Removal from Water by Adsorption on Geomaterial, Activated Carbon and Clay Adsorbents. *Ecol. Chem. Eng. S* **2021**, *28*, 303–328. [CrossRef]

31. Adsorbent, C.M.; Bruckmann, S.; Schnorr, C.E.; Salles, R.; Nunes, F.B.; Baumann, L.; Müller, E.I.; Silva, L.F.O.; Dotto, G.L.; Rodrigo, C.; et al. Highly Efficient Adsorption of Tetracycline Using. *Polymers* **2022**, *14*, 4854. [CrossRef] [PubMed]
32. Bao, J.; Zhu, Y.; Yuan, S.; Wang, F.; Tang, H.; Bao, Z.; Zhou, H.; Chen, Y. Adsorption of Tetracycline with Reduced Graphene Oxide Decorated with $MnFe_2O_4$ Nanoparticles. *Nanoscale Res. Lett.* **2018**, *13*, 396. [CrossRef]
33. Dong, Y.; Yi, C.; Yang, S.; Wang, J.; Chen, P.; Liu, X.; Du, W.; Wang, S.; Liu, B.F. A Substrate-Free Graphene Oxide-Based Micromotor for Rapid Adsorption of Antibiotics. *Nanoscale* **2019**, *11*, 4562–4570. [CrossRef] [PubMed]
34. Xiong, W.; Zeng, G.; Yang, Z.; Zhou, Y.; Zhang, C.; Cheng, M.; Liu, Y.; Hu, L.; Wan, J.; Zhou, C.; et al. Adsorption of Tetracycline Antibiotics from Aqueous Solutions on Nanocomposite Multi-Walled Carbon Nanotube Functionalized MIL-53(Fe) as New Adsorbent. *Sci. Total Environ.* **2018**, *627*, 235–244. [CrossRef]
35. Ahamad, T.; Ruksana; Chaudhary, A.A.; Naushad, M.; Alshehri, S.M. Fabrication of $MnFe_2O_4$ Nanoparticles Embedded Chitosan-Diphenylureaformaldehyde Resin for the Removal of Tetracycline from Aqueous Solution. *Int. J. Biol. Macromol.* **2019**, *134*, 180–188. [CrossRef]
36. Ren, X.; Yang, L.; Liu, M. Kinetic and Thermodynamic Studies of Acid Scarlet 3r Adsorption onto Low-Cost Adsorbent Developed from Sludge and Straw. *Chinese J. Chem. Eng.* **2014**, *22*, 208–213. [CrossRef]
37. WANG, C.; JIAN, J.-J. Degradation and Detoxicity of Tetracycline by an Enhanced Sonolysis. *J. Water Environ. Technol.* **2015**, *13*, 325–334. [CrossRef]
38. Mahmoud, A.A.; Osman, O.; Eid, K.; Alashkar, E.; Okasha, A.; Atta, D.; Eid, M.; Aziz, Z.A.; Fakhry, A. FTIR Spectroscopy of Natural Bio-Polymers Blends. *Appl. Sci.* **2014**, *4*, 816–824.
39. Salam, M.A.; Burk, R. Synthesis and Characterization of Multi-Walled Carbon Nanotubes Modified with Octadecylamine and Polyethylene Glycol. *Arab. J. Chem.* **2017**, *10*, S921–S927. [CrossRef]
40. Osler, K.; Twala, N.; Oluwasina, O.O.; Daramola, M.O. Synthesis and Performance Evaluation of Chitosan/Carbon Nanotube (Chitosan/MWCNT) Composite Adsorbent for Post- Combustion Carbon Dioxide Capture. *Energy Procedia* **2017**, *114*, 2330–2335. [CrossRef]
41. Rahmani, O.; Bouzid, B.; Guibadj, A. Extraction and Characterization of Chitin and Chitosan: Applications of Chitosan Nanoparticles in the Adsorption of Copper in an Aqueous Environment. *E-Polymers* **2017**, *17*, 383–397. [CrossRef]
42. Wei, J.; Yan, L.; Zhang, Z.; Hu, B.; Gui, W.; Cui, Y. Carbon Nanotube/Chitosan Hydrogel for Adsorption of Acid Red 73 in Aqueous and Soil Environments. *BMC Chem.* **2023**, *17*, 104. [CrossRef]
43. Gao, F.; Xu, Z.; Dai, Y. Removal of Tetracycline from Wastewater Using Magnetic Biochar: A Comparative Study of Performance Based on the Preparation Method. *Environ. Technol. Innov.* **2021**, *24*, 101916. [CrossRef]
44. Jayakumar, R.; Prabaharan, M.; Nair, S.V.; Tamura, H. Novel Chitin and Chitosan Nanofibers in Biomedical Applications. *Biotechnol. Adv.* **2010**, *28*, 142–150. [CrossRef]
45. Zhang, L.; Xia, Z. Mechanisms of Oxygen Reduction Reaction on Nitrogen-Doped Graphene for Fuel Cells. *J. Phys. Chem. C* **2011**, *115*, 11170–11176. [CrossRef]
46. Sobh, R.A.; Nasr, H.E.S.; Mohamed, W.S. Formulation and in Vitro Characterization of Anticancer Drugs Encapsulated Chitosan/Multi-Walled Carbon Nanotube Nanocomposites. *J. Appl. Pharm. Sci.* **2019**, *9*, 32–40. [CrossRef]
47. Lv, W.; Shi, K.; Li, L.; Shao, S. Nitrogen-Doped Multiwalled Carbon Nanotubes and Their Electrocatalysis towards Oxidation of NO. *Microchim. Acta* **2010**, *170*, 91–98. [CrossRef]
48. Mkhondo, N.B.; Magadzu, T. Effects of Different Acid-Treatment on the Nanostructure and Performance of Carbon Nanotubes in Electrochemical Hydrogen Storage. *Dig. J. Nanomater. Biostructures* **2014**, *9*, 1331–1338.
49. Barrett, E.P.; Joyner, L.G.; Halenda, P.P. The Determination of Pore Volume and Area Distributions in Porous Substances. I. Computations from Nitrogen Isotherms. *J. Am. Chem. Soc.* **1951**, *73*, 373–380. [CrossRef]
50. Pillai, C.K.S.; Paul, W.; Sharma, C.P. Chitin and Chitosan Polymers: Chemistry, Solubility and Fiber Formation. *Prog. Polym. Sci.* **2009**, *34*, 641–678. [CrossRef]
51. Jin, J.; Yang, Z.; Xiong, W.; Zhou, Y.; Xu, R.; Zhang, Y.; Cao, J.; Li, X.; Zhou, C. Cu and Co Nanoparticles Co-Doped MIL-101 as a Novel Adsorbent for Efficient Removal of Tetracycline from Aqueous Solutions. *Sci. Total Environ.* **2019**, *650*, 408–418. [CrossRef]
52. Zhao, W.; Hao, C.; Guo, Y.; Shao, W.; Tian, Y.; Zhao, P. Optimization of Adsorption Conditions Using Response Surface Methodology for Tetracycline Removal by MnFe2O4/Multi-Wall Carbon Nanotubes. *Water* **2023**, *15*, 2392. [CrossRef]
53. Li, R.; Zhang, Y.; Deng, H.; Zhang, Z.; Wang, J.J.; Shaheen, S.M.; Xiao, R.; Rinklebe, J.; Xi, B.; He, X.; et al. Removing Tetracycline and Hg(II) with Ball-Milled Magnetic Nanobiochar and its Potential on Polluted Irrigation Water Reclamation. *J. Hazard. Mater.* **2020**, *384*, 121095. [CrossRef] [PubMed]
54. Deng, R.; Huang, D.; Zeng, G.; Wan, J.; Xue, W.; Wen, X.; Liu, X.; Chen, S.; Li, J.; Liu, C.; et al. Decontamination of Lead and Tetracycline from Aqueous Solution by a Promising Carbonaceous Nanocomposite: Interaction and Mechanisms Insight. *Bioresour. Technol.* **2019**, *283*, 277–285. [CrossRef]
55. Khodaie, M.; Ghasemi, N.; Moradi, B.; Rahimi, M. Removal of Methylene Blue from Wastewater by Adsorption onto Znclactivated Corn Husk Carbon Equilibrium Studies. *J. Chem.* **2013**, *2013*, 383985. [CrossRef]

56. Laysandra, L.; Ondang, I.J.; Ju, Y.H.; Ariandini, B.H.; Mariska, A.; Soetaredjo, F.E.; Putro, J.N.; Santoso, S.P.; Darsono, F.L.; Ismadji, S. Highly Adsorptive Chitosan/Saponin-Bentonite Composite Film for Removal of Methyl Orange and Cr(VI). *Environ. Sci. Pollut. Res.* **2019**, *26*, 5020–5037. [CrossRef]
57. Ranjbari, S.; Tanhaei, B.; Ayati, A.; Khadempir, S.; Sillanpää, M. Efficient Tetracycline Adsorptive Removal Using Tricaprylmethylammonium Chloride Conjugated Chitosan Hydrogel Beads: Mechanism, Kinetic, Isotherms and Thermodynamic Study. *Int. J. Biol. Macromol.* **2020**, *155*, 421–429. [CrossRef]
58. Paula Fagundes, A.; Felipe Viana da Silva, A.; Bueno de Morais, B.; Lusitâneo Pier Macuvele, D.; Nones, J.; Gracher Riella, H.; Padoin, N.; Soares, C. A Novel Application of Bentonite Modified with Copper Ions in the Tetracycline Adsorption: An Experimental Design Study. *Mater. Lett.* **2021**, *291*, 129552. [CrossRef]
59. Le, T.T.N.; Le, V.T.; Dao, M.U.; Nguyen, Q.V.; Vu, T.T.; Nguyen, M.H.; Tran, D.L.; Le, H.S. Preparation of Magnetic Graphene Oxide/Chitosan Composite Beads for Effective Removal of Heavy Metals and Dyes from Aqueous Solutions. *Chem. Eng. Commun.* **2019**, *206*, 1337–1352. [CrossRef]
60. Istiningrum, R.B.; Tiwow, C.D.; Nuryono; Narsito. Au(III) Selective Adsorption of Quaternary Ammonium-Silica Hybrid in Au/Cu System. *Procedia Chem.* **2015**, *17*, 132–138. [CrossRef]
61. Zhou, J.; Zhou, X.; Yang, K.; Cao, Z.; Wang, Z.; Zhou, C.; Baig, S.A.; Xu, X. Adsorption Behavior and Mechanism of Arsenic on Mesoporous Silica Modified by Iron-Manganese Binary Oxide (FeMnOx/SBA-15) from Aqueous Systems. *J. Hazard. Mater.* **2020**, *384*, 121229. [CrossRef]
62. Kumar, P.S.; Ramalingam, S.; Sathyaselvabala, V.; Kirupha, S.D.; Murugesan, A.; Sivanesan, S. Removal of Cadmium(II) from Aqueous Solution by Agricultural Waste Cashew Nut Shell. *Korean J. Chem. Eng.* **2012**, *29*, 756–768. [CrossRef]
63. Zhang, Z.; Ding, C.; Li, Y.; Ke, H.; Cheng, G. Efficient Removal of Tetracycline Hydrochloride from Aqueous Solution by Mesoporous Cage MOF-818. *SN Appl. Sci.* **2020**, *2*, 669. [CrossRef]
64. Uzun, I.; Güzel, F. Kinetics and Thermodynamics of the Adsorption of Some Dyestuffs and P-Nitrophenol by Chitosan and MCM-Chitosan from Aqueous Solution. *J. Colloid Interface Sci.* **2004**, *274*, 398–412. [CrossRef]
65. Liu, T.; Li, Y.; Du, Q.; Sun, J.; Jiao, Y.; Yang, G.; Wang, Z.; Xia, Y.; Zhang, W.; Wang, K.; et al. Adsorption of Methylene Blue from Aqueous Solution by Graphene. *Colloids Surf. B Biointerfaces* **2012**, *90*, 197–203. [CrossRef] [PubMed]
66. Al-Kindi, G.Y.; Alnasrawy, S.T. Tetracycline Remove from Synthetic Wastewater by Using Several Methods. *J. Ecol. Eng.* **2022**, *23*, 137–148. [CrossRef]
67. Yang, K.; Lou, Z.; Fu, R.; Zhou, J.; Xu, J.; Baig, S.A.; Xu, X. Multiwalled Carbon Nanotubes Incorporated with or without Amino Groups for Aqueous Pb(II) Removal: Comparison and Mechanism Study. *J. Mol. Liq.* **2018**, *260*, 149–158. [CrossRef]
68. Kumar, R.; Ansari, M.O.; Barakat, M.A. DBSA Doped Polyaniline/Multi-Walled Carbon Nanotubes Composite for High Efficiency Removal of Cr(VI) from Aqueous Solution. *Chem. Eng. J.* **2013**, *228*, 748–755. [CrossRef]
69. Gupta, V.K.; Chandra, R.; Tyagi, I.; Verma, M. Removal of Hexavalent Chromium Ions Using CuO Nanoparticles for Water Purification Applications. *J. Colloid Interface Sci.* **2016**, *478*, 54–62. [CrossRef] [PubMed]
70. Piccin, J.S.; Dotto, G.L.; Pinto, L.A.A. Adsorption Isotherms and Thermochemical Data of FDandC RED N° 40 Binding by Chitosan. Brazilian *J. Chem. Eng.* **2011**, *28*, 295–304. [CrossRef]